Mineralogical Characterisation to improve understanding of oral bioaccessibility of Cr and Ni in Basaltic Soils in Northern Ireland

Cox, S., McKinley, J., & Rollinson, G. (2017). Mineralogical Characterisation to improve understanding of oral bioaccessibility of Cr and Ni in Basaltic Soils in Northern Ireland. *Journal of Geochemical Exploration*, *183*, 166–177. https://doi.org/10.1016/j.gexplo.2017.02.006

Published in:
Journal of Geochemical Exploration

Document Version:
Peer reviewed version

Queen's University Belfast - Research Portal:
Link to publication record in Queen's University Belfast Research Portal

MINERALOGICAL CHARACTERISATION TO IMPROVE UNDERSTANDING OF ORAL BIOACCESSIBILITY OF Cr AND Ni IN BASALTIC SOILS IN NORTHERN IRELAND

Siobhan F. Cox [a*], Gavyn Rollinson [b] and Jennifer M. McKinley [a]

[a] School of Natural and Built Environment, Queen's University Belfast, Belfast, BT9 5AG, UK.
s.cox@qub.ac.uk

[b] Camborne School of Mines, College of Engineering, Mathematics & Physical Sciences, University of Exeter, Penryn Campus, Cornwall, TR10 9FE, UK. G.K.Rollinson@exeter.ac.uk

[c] School of Natural and Built Environment, Queen's University Belfast, BT7 1NN, UK.
j.mckinley@qub.ac.uk

*Address correspondence to Siobhan Cox, School of Natural and Built Environment, Queen's University Belfast, Belfast, BT9 5AG, UK Phone:+44 28 9097 4152, Fax:+44 28 9097 4278;
E-mail:s.cox@qub.ac.uk

ABSTRACT

Underlying bedrock is often the source of elevated levels of potentially toxic elements (PTEs) (including Ni and Cr) in soils, which can be at concentrations exceeding regulatory guidelines for the protection of human health. However geogenic contaminants are often not significantly bioavailable to humans as they are bound tightly within the soil matrix. Therefore oral bioaccessibility testing can be used to refine human health risk assessment by quantifying bioaccessible PTEs in soils, but should be augmented with soil mineralogy data to support its use in risk assessment. Elemental mapping using Electro Probe Microanalysis (EPMA) and mineralogical mapping using QEMSCAN®, an automated mineral/phase analysis system based on a scanning electron microscope, were combined with quantitative X-Ray Diffraction (XRD) and previous oral bioaccessibility and non-specific sequential extraction (CISED) results for 3 soil samples overlying Palaeogene basalt lavas in Northern Ireland, to determine the effect of soil mineralogy on oral bioaccessibility of Ni and Cr. Results indicate that Cr concentrations are principally related to recalcitrant chrome spinel and primary iron oxides, which explains the relatively low bioaccessibility of Cr. In contrast, Ni is more widely dispersed within the soils, with a proportion of total Ni found in carbonates and weathering products, including secondary iron oxides and precursor clay minerals, leading to the higher oral bioaccessibility measurements recorded for Ni than Cr.

Suggested keywords

Nickel, Chromium, Oral bioaccessibility, Basalt, Mineralogical analysis, Elemental mapping

Graphical abstract

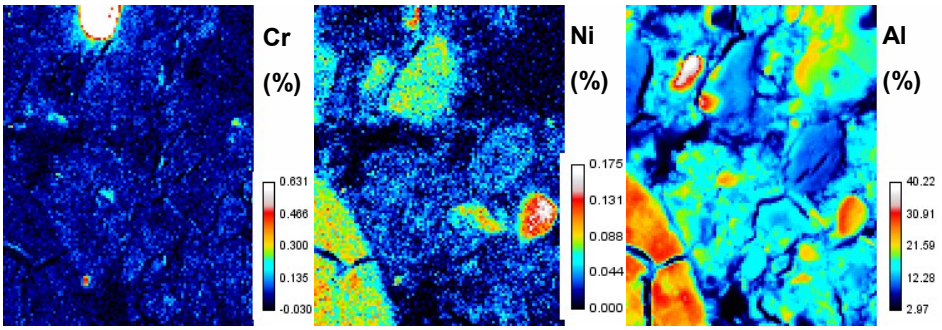

Highlights

- Ni and Cr analysis of Basaltic soils overlying Antrim Basalts of Northern Ireland
- Combined chemical and mineralogical data for improved understanding
- High resolution analysis of samples, consistent across analytical methods
- Bioaccessible Ni in precursor clay minerals, secondary Fe-oxides and carbonates
- Low Cr bioaccessibility as Cr predominantly in chrome spinel and primary Fe-oxides

Abbreviations

BAF	Bioaccessible Fraction
BARGE	Bioaccessibility Research Group of Europe
BSE	Backscattered Electron
CISED	Non-specific Sequential Extraction coupled with Chemometric Analysis
CTM	Causeway Tholeiite Member
EDS	Energy Dispersive Spectrometer
EPMA	Electron Probe Micro Analyser
G	Gastric Phase
GI	Gastrointestinal Phase
LBF	Lower Basalt Formation
LOI	Loss on Ignition
PTE	Potentially Toxic Element

62	QEMSCAN	Quantitative Evaluation of Minerals by Scanning Electron Microscopy
63	S4UL	Suitable for Use Level
64	SDD	Silicon Drift Detector
65	SEM	Scanning Electron Microscope
66	SGV	Soil Guideline Value
67	SOC	Soil Organic Carbon
68	UBF	Upper Basalt Formation
69	UBM	Unified BARGE Method
70	WDS	Wavelength Dispersive Spectrometers
71	XRD	X-Ray Diffraction
72	XRFS	X-ray Fluorescence

73

1.0 INTRODUCTION

Elevated concentrations of nickel (Ni) and chromium (Cr) from both geogenic and anthropogenic sources have been identified in soils throughout the world including Canada (Vasiluk et al., 2011), Brazil (Colin et al., 1990), the Czech Republic (Quantin et al., 2008), Poland (Kierczak et al., 2007), Portugal (Costa et al., 2011), UK (Barsby et al., 2012; Palmer et al., 2014; Wragg et al., 2014), Italy (Albanese et al., 2015) and Greece (Albanese et al., 2015; Argyraki and Kelepertzis, 2014; Kelepertzis and Stathopoulou, 2013). Total concentrations of these elements are often at levels exceeding regulatory guidelines suggesting they may potentially cause harm to human health. Recently this has been compounded by new toxicological advice (EFSA, 2015) which indicates that tolerable daily intakes of oral Ni are lower than was assumed in derivation of many of these guideline values. On this basis the Environment Agency in England and Wales withdrew the Soil Guideline Value (SGV) for nickel in 2015 and a new "suitable for use level" (S4UL) for Ni of 130mg kg^{-1} was published by Nathanail et al. (2015) for a residential land use that includes the production of home-grown produce. S4ULs indicate a level of minimal or tolerable level of risk, indicating a site is suitable for the land use the S4UL has been derived for (Nathanail et al., 2015). Concentrations of PTEs above S4ULs may require further assessment of risks to determine if any remedial action is required.

However, total concentrations do not reflect the amount of a contaminant that is actually bioavailable to humans via the oral, inhalation and dermal pathways (Ruby et al., 1999). The use of oral bioaccessibility testing provides risk assessors with an estimation of the amount of an element that will

become dissolved in the gastro intestinal tract (and is therefore accessible to humans via the oral pathway), allowing assessors to more accurately consider potential risks posed to human health. The Unified BARGE Method (UBM) was developed by the BARGE (Bioaccessibility Research Group of Europe) research group (Wragg et al., 2011) and has been validated against in vivo studies for As, Pb and Cd (Denys et al., 2012). However , as oral bioaccessibility can be affected by a number of factors including mineralogy, particle size, solid-phase speciation and encapsulation (Cave et al., 2011; Ruby et al., 1999), a "lines of evidence" approach (CIEH, 2009) is recommended to support oral bioaccessibility testing, utilising information relating to soil mineralogy and the mobility and distribution of the contaminant in the soil.

McIlwaine et al. (2014) used data from the Tellus Geochemical Survey of Northern Ireland (Smyth, 2007) and geological mapping to identify domains (areas where a readily identifiable factor can be shown to control the concentration of an element) for a number of PTEs in Northern Ireland. Soils overlying the Antrim Lava Group were identified as a domain with elevated Ni and Cr, with median Ni concentrations in the domain being were approximately 4 times greater for Ni and 2.5 times greater for Cr than the rest of Northern Ireland. However oral bioaccessisbility testing undertaken by (Barsby et al., 2012; Palmer et al., 2014) indicate the oral bioaccessibility of Cr and Ni in these soils is quite low (Cr < 5.5%; Ni < 44%). Investigations undertaken by Cox et al. (2013) found that bioaccessible Cr in the basaltic soils of Northern Ireland is strongly correlated with total Cr and Fe_2O_3, indicating that Cr is predominantly present in phases associated with Fe_2O_3 that have relatively low bioaccessibility.

Non-specific sequential extractions (CISED), showed that the majority of Cr was present in oxides, with a only a very small component present in clays (Cox et al., 2013). In contrast Cox et al. (2013) found that bioaccessible Ni (both G and GI) was not strongly correlated with total Ni, most of the major oxides or Soil Organic Carbon (SOC). Indeed, CISED extractions showed that bioaccessible Ni was related to all identified soil components, including calcium carbonate, aluminium oxide, iron oxide and clay-related components, suggesting weathering significantly affects nickel bioaccessibility but has a less significant role in the bioaccessibility of Cr in these soils (Cox et al., 2013). However, without detailed data relating specifically to soil mineralogy and element distribution within the soils, interpretation of the role of mineralogy on the oral bioaccessibility of Ni and Cr was incomplete.

The aim of this research is to further investigate the controls on oral bioaccessibility of PTEs in Ni and Cr rich soils overlying the Antrim Basalts in Northern Ireland to provide evidence to support the use of oral bioaccessibility testing both in Northern Ireland and internationally. To meet this aim: 1) the mineralogy of soils overlying the Antrim Basalts is characterised using both quantitative XRD and QEMSCAN® analyses combined with detailed geochemical data; 2) detailed elemental and mineralogical mapping are compared to determine which minerals host total Ni and Cr; and 3) this information is related to results of previous bioaccessibility testing (Barsby et al., 2012) and non-specific sequential extractions (Cox et al., 2013) to elucidate how the oral bioaccessibility of both Ni and Cr is affected by soil composition.

2.0 MATERIALS AND METHODS

2.1 Study area

The Antrim Lava Group was formed in two cycles of volcanic activity that occurred about 60 million years ago (Lyle, 1979). It extends across the north eastern corner of Northern Ireland (Figure 1), covering an area of 4009 km^2 (Cruickshank, 1997). The first cycle of volcanic activity produced olivine theoleiite lavas that formed the Lower Basalt Formation (LBF), whilst fractionation of this magma gave rise to intermediate lavas towards the top of the Lower Basalts (Mitchell, 2004). The second cycle of volcanic activity, approximately 5 million years later, formed the Upper Basalt Formation (UBF) (also olivine theoleiites) (Mitchell, 2004). In the period between the formation of the Upper and Lower Basalts, a period of extensive chemical weathering of the Lower Basalts occurred, which resulted in the formation of the Interbasaltic Formation comprising of deeply weathered and lateritised basalts that are found between the Upper and Lower Basalt Formations (Hill et al., 2001). Also during the period between the cycles of volcanic activity that formed the Upper and Lower Basalts, eruption of the mainly quartz tholeiites of the Causeway Tholeite Member (CTM)) occurred (Mitchell, 2004). The Upper and Lower Basalts are composed principally of plagioclase feldspars (labradorite), Mg-rich olivine containing small spinal inclusions and pyroxene (augite) (Lyle, 1979) with magnetite, ilmenite and apatite also present as accessory minerals (Hill et al., 2001).

152 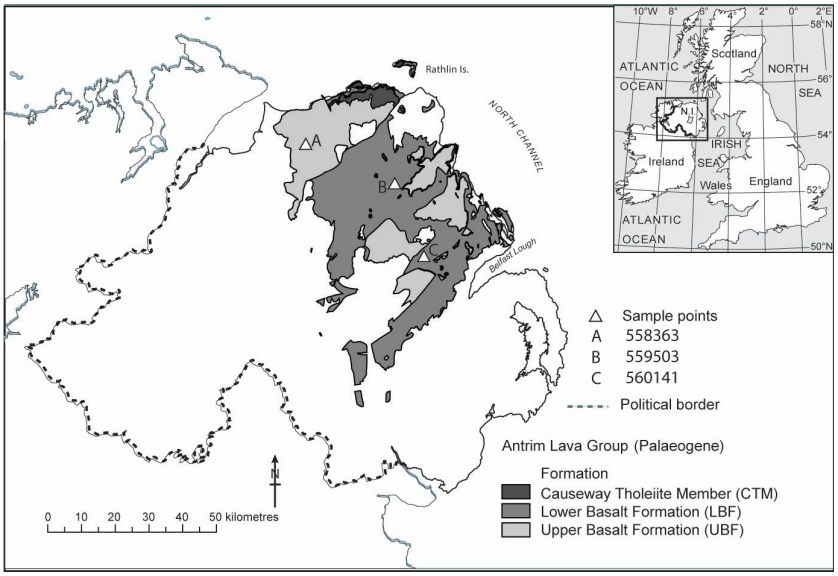

153 **Figure 1 Map showing the Antrim Lava Group.**

154

155 Figure 2a shows the spatial distribution of total Ni concentrations determined during the Tellus survey.

156 Median total Ni concentrations in the UBF and LBF were 100 mg kg^{-1}, with the highest Ni concentration

157 recorded in the Tellus Survey (334 mg kg^{-1}) reported for the LBF (Cox et al., 2013). 516 samples

158 overlying the Antrim Basalts (31%) have total Ni concentrations that exceed the "Suitable for Use Level"

159 (S4UL) for Ni (130 mg kg^{-1}) for a residential landuse (with homegrown produce) derived by Nathanail et

160 al. (2015).

161

162 Similar trends are observed for total Cr concentrations (Fig. 2b), which are generally about 3 to 4 times

163 greater than total Ni concentrations (Cox et al., 2013). Cr speciation was not determined during the

164 Tellus survey, so both the S4UL for Cr (III) and Cr (VI) have been used for comparison. All samples

165 from the study area (1664 samples; 100%) have total Cr concentrations that exceed the residential S4UL

166 for Cr VI of 6 mg kg^{-1}, whilst 3 samples (0.18%) exceed the residential with gardens S4UL for Cr III of

167 910 mg kg^{-1}.

168

169 Cox et al., (2013) reported that bioaccessible Ni and Cr were generally greater in gastric phase extracts

170 than in the gastrointestinal phase, with samples overlying the LBF containing the greatest amount of

171 bioaccessible Ni (mean gastric phase concentration of 6.17 mg kg^{-1}), while the UBF showed greater

172 amounts of bioaccessible Cr (mean gastric phase concentration of 4.55 mg kg^{-1}). Ni and Cr

173 bioaccessible fraction (BAF) was also greater in the gastric phase than in the gastrointestinal phase, with

174 Ni BAFs being up to 8 times greater than Cr BAF.

175

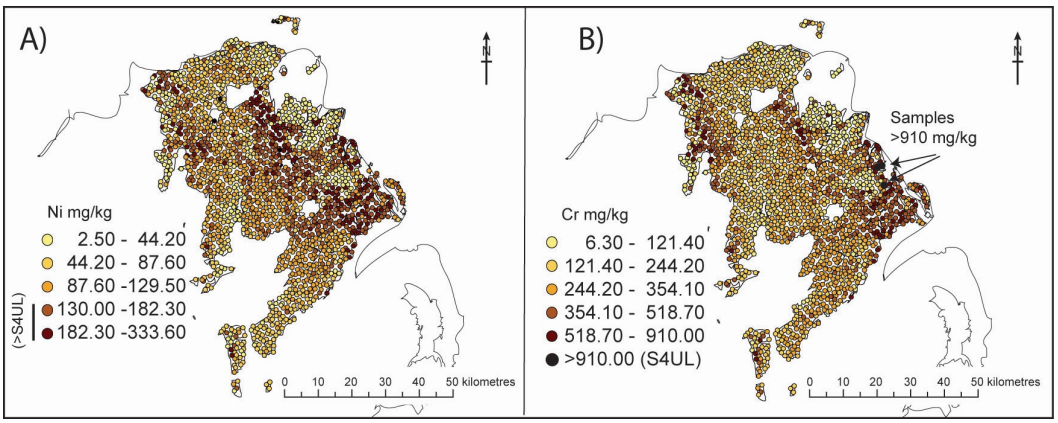

176

177 **Figure 2 Maps showing the spatial distribution of (A) total Ni and (B) total Cr (by XRF (mg kg^{-1}))**

178 **for all Tellus soil samples overlying the Antrim Lava Group**

179

180

2.2 Collection, preparation and soil analyses

During the Tellus geochemical survey, samples were disaggregated and sieved to a <2 mm fraction (Smyth, 2007), prior to being analysed for a range of elements and major oxides using X-ray fluorescence (XRFS) as well as pH and soil organic carbon (SOC) (Smyth 2007). Barsby et al., (2012) reported the results of oral bioaccessibility testing for these samples using the Unified BARGE Method (UBM) (Denys et al., 2012; Wragg et al., 2011). Both the actual bioaccessibility of PTEs (mg kg^{-1}) and the bioaccessible fraction (BAF) (the ratio of bioaccessible concentration from the UBM test and total concentration by XRFS), are reported in the gastric and gastrointestinal phase to allow discussion of all four measurements. Quality control procedures employed for XRFS, pH and LOI analyses are presented in Smyth (2007), and Barsby et al., (2012) provides full details of the use of reference materials, duplicates and blanks for UBM testing.

Three sieved and dried surface soil samples (558363, 559503, 560141), retrieved from areas overlying the Antrim Lava Group were recovered from the Tellus archive for quantitative XRD analyses and mineralogical and elemental mapping. For optical and e-beam microscopy, two samples (558363, 559503) were prepared as polished thin sections by embedding in epoxy resin followed by grinding and polishing to 30 μm thickness with ethane diol and aluminium oxide, with final cleaning undertaken using alcohol. A third sample (560141) was prepared as a 30 mm diameter epoxy mount, and polished to a 1 micron finish using diamond media. For e-beam analysis, all samples were carbon coated with approximately a 25 nm layer of carbon, to allow the electron beam to conduct across the sample surface.

201

202 **2.3 Quantitative XRD analysis**

203 Quantitative XRD analysis was undertaken by X-Ray Mineral Services Colywn Bay, UK, using a Philips:
204 PW1730 X-ray Generator, with copper anode tube equipped with a Philips PW1050 Goniometer and
205 graphite monochromator.

206

207 ***2.3.1 Whole (Bulk) Rock Analysis***

208 Samples were disaggregated using a pestle and mortar and 'micronised' using a McCrone Micronising
209 Mill to obtain a mean particle diameter of between 5 - 10 microns. This was mixed with water and the
210 resulting slurry was dried overnight at 80°C, re-crushed and homogenised to a fine powder and
211 back-packed into an aluminium cavity mount, producing a randomly orientated sample for presentation
212 to the x-ray beam.

213

214 Samples were analysed between 2° and 70° 2θ (theta) with a step size of 0.05°/sec using x-ray radiation
215 from a copper anode at 35kV, 30mA . X-Ray Mineral Services "Traces" and "Search-Match" software
216 was used to compare the x-ray diffraction pattern from the unknown sample with the International Centre
217 for Diffraction Data PDF-4 Minerals database to identify unknown minerals. Amorphous content was
218 calculated by spiking with silicon (metal powder) and Siroquant software was used to quantify phases
219 identified in each sample.

220

2.3.2 Clay Mineral analysis

The <2 micron fraction of a 5 gram split of disaggregated sample, was separated by ultrasound, shaking and centrifugation. The total weight of clay extracted was determined by removing a 20ml aliquot of the final clay suspension and evaporating to dryness at 80°C. Clay XRD mounts were obtained by filtering the clay suspension through a Millipore glass microfiber filter and drying the filtrate on the filter paper. The samples were analysed as an untreated clay, after saturation with ethylene glycol vapour overnight and following heating at 380°C for 2 hours and 550°C for one hour. The initial scan for these four treatments was between 3° and 35° 2θ (theta) at a step size of 0.05°/sec using x-ray radiation from a copper anode at 40kV, 30mA. The untreated sample was also analysed between 24-27° 2θ at a step size of 0.02 °/2 sec to further define kaolinite/chlorite peaks.

Diffractograms from the four clay treatments were overlain to identify the clay mineral assemblages present. Peak intensities were measured to calculate the relative amounts of clay minerals present, which were subsequently used to quantify the clay minerals with respect to the whole rock by reference to the total amount of <2 micron clay fraction. An indication of the clay minerals crystallinity was given by assessment of the peak width for each component.

2.4 Mineralogical mapping

Mineralogical mapping was undertaken using QEMSCAN®, an automated mineral/phase analysis system based on a scanning electron microscope (SEM) that provides rapid determination and quantification of

241 the mineralogy, chemical composition (through defined databases) and grain size of a sample (Gottlieb et
242 al., 2000; Haberlah et al., 2011). QEMSCAN® is a mature technique that is over 40 years old and has
243 been used in a variety of research projects (Pirrie and Rollinson, 2011; Santoro et al., 2014). Analysis
244 was undertaken at the Camborne School of Mines, University of Exeter, using a QEMSCAN® 4300
245 system.
246
247 During QEMSCAN® analysis an electron beam is rastered across the sample surface producing a
248 Backscattered Electron (BSE) image and X-rays which are used to identify the mineralogy. For this
249 investigation, samples were analysed using the Fieldscan mode using iMeasure software, which
250 measured each sample in fields (1.5mm squares) at a 10 μm X-ray pixel spacing, with the resin media
251 ignored due to being below a pre-set BSE threshold. Data processing was undertaken using iDiscover
252 software, which is an involved process that requires checks of the mineral database and refinement of the
253 data specific to the context of the sample type. The resultant fields are then recombined (stitched) to
254 give an overall false colour mineral map with corresponding data tables for mineral abundances and
255 associations. The advantage of Fieldscan mode was that it examined the entire sample area providing
256 excellent spatial modal mineralogy with between 1.3 and 2.4 million analysis points. However, pixel
257 resolution was carefully designed to avoid excessive measurement time, thus minerals or textures less
258 than the pixel resolution (10 microns) are poorly represented but compensated for by the BSE and
259 element maps. The advantages and limitations of the QEMSCAN® technique are discussed in detail in
260 Andersen et al. (2009) and Rollinson et al. (2011).

Standard operating conditions were 25kV and 5nA using a tungsten filament operating under a customized high vacuum. X-ray collection rate was 1000 counts combined from four EDS Bruker Silicon Drift (SDD) detectors, with a maximum X-ray resolution of around 1 micron. Operation of QEMSCAN® followed quality control procedures developed at the Camborne School of Mines, University of Exeter, for sample preparation, instrument calibration, operation and data processing. See Rollinson et al. (2011) for further details.

Minerals with similar chemical composition were grouped together and groups were described either by the elemental composition, or in some cases the minerals deemed most likely to be present as shown in Table 1. QEMSCAN® cannot separate polymorphs (minerals with the same chemistry but different crystallography) as its analysis is based on chemical spectra and minerals/phases with very similar or overlapping chemical spectra can be difficult to separate. Very fine grained material such as mixed clays (less than 5 microns) may also be difficult to separate chemically due to the beam excitation volume effects (Rollinson et al., 2011) and only elements that are greater than approx. 3% in concentration at each analysis point may be detected (Andersen et al., 2009). Total percentages for each mineral group reported here, have been corrected to include soil organic carbon (SOC) as measured during the Tellus survey, as SOC is not quantified by QEMSCAN® analysis.

Mineral Category	Mineral Description
Background	All resin/mounting media and related edge effects

Chrome spinel	Includes any phase with Cr, Fe, Al and Mg; such as Chromite, Chrome metal and Chrome Spinel
Fe Ox/CO_3	Fe oxides and carbonates such as Siderite, Hematite, Magnetite, Ti-Magnetite, Fe Metal and any other Fe-Oxide/Carbonate.
Mn phases	Includes Mn Silicates and Mn Fe Oxides
Rutile	Any phase with Ti and O; includes Rutile/Anatase/Brookite
Ilmenite	Any phase with Fe, Ti and O
Zircon	Any phase with Zr, Si and O
REE phases	Includes Monazite (Ce Phosphates)
Quartz	Quartz and other silica minerals
Plagioclase feldspar	Plagioclase Feldspars: phases with Na, Al, Si and O to Ca, Al, Si and O. May include a boundary effect with Quartz and Al oxide polishing media (mixed spectra looks like Albite)
K-Feldspar	Any phase with K, Al, Si and O; includes Orthoclase/Microcline/Sanidine
Muscovite/Illite	Muscovite Mica, may include Illite (K, Al, Si and O)
Fe Al K silicates	Any phase with Fe, Al, K and Si; such as Biotite Mica and any other Mica except Muscovite, may include Glauconite
Mg + Fe silicates	Any phase with Mg, Fe and Si; such as Olivine, Talc, Serpentine Group, includes Fe Silicates
Ca Mg Fe silicates	Any phase with Ca, Mg, Fe and Si (with or without Fe and Al); such as Hornblende, Tremolite, Augite, Diopside, Actinolite, maybe Amphiboles and Pyroxenes
Al silicates (excluding kaolinite)	Any phase with Al, Si and O; separated from Kaolinite by the Al-Si ratio. May contain low amounts of other elements such as Fe, Mg and Ca. May contain Albite
Kaolinite	Al silicates such as Kaolinite/Halloysite/Dickite and Topaz, and any other Al silicate
Fe Al (Mg) silicates	Any phase with Fe, Al and Si, with or without Mg; such as Chlorite/ Clinochlore, Nontronite, Vermiculite
Calcite	Any phase with Ca, O and C
Apatite	Apatite and any other Ca Phosphates
Others	Any other mineral not included above. Boundary/polishing effects

Table 1 Mineral groupings used for reporting results of QEMSCAN® analysis

2.5 Elemental mapping

Elemental analysis and mapping was undertaken at the School of Earth Sciences, University of Bristol using a JEOL JXA8530F electron probe microanalyser (EPMA), equipped with both a silicon drift detector (SSD) energy dispersive spectrometer (EDS) and 5 wavelength dispersive spectrometers (WDS). Results from the QEMSCAN® analysis were used to identify locations for quantitative element point analysis and areas for elemental mapping on each of the three samples. Point locations included

representative examples of chrome spinel, iron oxide, calcite and apatite. Mapping was targeted on areas of typical clay composition and where it was suspected olivine was weathering within the basalt. Quantitative analysis of elemental concentrations was undertaken by WDS. Details of EPMA setup are summarised in Table 2.

	Major and trace elements (stable mineralogy)	Major elements (unstable mineralogy)	Trace elements (unstable mineralogy)	Major and trace elements (apatite)	Major and trace elements (calibration of maps 0043, 0059, 0061 and 0063)	Major and trace elements (calibration of maps 0029-0032)
Acceleration voltage (kV)	20	20	20	20	20	20
Probe current (nA)	40	2	40	2	40	40
Beam size (µm)	1	10	1	15	1	1

Table 2 Acceleration voltages, probe currents, beam size and dwell times for quantitative analyses

The crystals and standards used were Al as Al_2O_3 (Amelia albite), Ca as CaO (Wollastonite), Cr as Cr_2O_3, Fe as FeO (Ilmenite), Mg as MgO (St John's Island Olivine), Mn as MnO, Na as Na_2O (Ameilia albite), P as P_2O_5 (Durango apatite), Si as SiO_2 (St John's Island Olivine), Ti as TiO_2 (Ilmenite), K as K_2O (Eifel sanidine); Ni and NiO, Zn as ZnO, V as V_2O_3 and Nb as Nb_2O_5 ($LiNbO_3$) and F as Durango apatite. V was measured using an overlap correction, which subtracts the overlapping Ti Kb component based on the intensity on the Ti Ka line.

303 The distribution of Mn, Ca, P, Mg, Ti, K, Si, Fe, Na, Al, Cr and Ni was determined using elemental

304 mapping. Mn, Ca, P, Mg, Ti, K, Si and Fe were mapped using EDS, and Na, Al, Cr and Ni were

305 mapped using WDS, with Ni mapped on two spectrometers. For the WDS elements a peak map and an

306 upper background map was collected providing net count maps. The EDS maps are total counts. The

307 maps were then calibrated using a calibration curve determined from a series of quantitative point

308 analyses undertaken within each mapping area. The size of the measured areas for each map are shown in

309 Table 3. All maps were measured with a step size of 1 µm.

310

Map No	Sample No	Width (µm)	Height (µm)	Step size (µm)
0029	558363	100	128	1
0030	558363	100	128	1
0031	559503	128	100	1
0032	559503	100	128	1
0043	558363	200	256	1
0059	560141	100	128	1
0061	560141	100	128	1
0063	560141	140	180	1

311 **Table 3 Measured area and step size for each elemental map**

312

313 **3.0 RESULTS AND DISCUSSION**

314 **3.1 Geochemical data**

315 Major element data (Table 4) shows that between 80 to 85% of the soils comprise Si, Al, Fe and SOC.

316 The contribution these elements make to the soil is similar between all three soils reflecting that they

317 overlie bedrock of similar origin. Ca and Mg are present in all soils at concentrations of approximately

318 2%, as would be expected given the presence of plagioclase feldspars and pyroxene in the underlying

319 bedrock (Lyle, 1979). Sample 560141 contained more Ca than the other 2 samples, which is consistent

with the results of non-specific sequential extractions on these soils by Cox et al. (2013).

	Sample 558363	Sample 559503	Sample 560141	Average compositions [1]			
				Basalt (n=5)	Lithomarge (n=126)	Laterite (n=99)	Iron crust (n=10)
SiO_2 %	39.60	39.50	43.40	43.94	37.33	21.54	12.72
TiO_2 %	1.56	1.37	1.08	1.87	2.64	3.99	9.99
$A1_2O_3$ %	13.10	14.70	13.50	15.15	27.86	33.78	17.51
Fe_2O_3 %	11.24	11.42	8.68	13.61	18.03	25.03	45.51
MnO %	0.22	0.27	0.11	0.34	0.18	0.1	0.06
MgO %	2.40	2.60	2.10	6.94	2.32	0.37	0.4
CaO %	1.76	2.53	3.10	9.32	1.8	0.45	0.59
Na_2O %	0.30	0.60	0.60	2.24	0.37	0.15	0.07
K_2O %	0.67	0.39	0.56	0.2	0.11	0.04	0.04
P_2O_5 %	0.32	0.56	0.41	0.15	0.2	0.13	0.07
SOC %	16.62	19.89	19.70	3.39	14.22	17.35	9.78
Ba (ppm)	238	207	250	53	87	81	248
Ce (ppm)	26	26	26	22	35	27	26
Cr (ppm)	448	300	293	205	384	572	832
Cu (ppm)	93	142	72	87	189	197	89
Nb (ppm)	8	8	9	3	6	18	74
Ni (ppm)	175	167	122	205	557	404	88
Pb (ppm)	21	16	22	<3	<3	6	10
Rb (ppm)	19	13	10	3	4	5	9
Sn (ppm)	3	2	3	<8	<8	< 8	<8
Sr (ppm)	42	82	116	233	87	30	67
Th (ppm)	2	2	2	<2	<2	4	13
U (ppm)	2	1	1	<2	<2	<2	3
V (ppm)	260	259	233	278	389	627	1227
Zn (ppm)	127	176	127	88	98	77	72
Zr (ppm)	166	106	95	84	90	142	173

Table 4 Geochemical composition of each soil sample (as determined by XRF analysis undertaken during the TELLUS survey) and averages geochemical composition for fresh and altered Antrim basalt. [1] Average concentrations of the main horizons within the laterite profile (Hill et al., 2001)

Comparison of the geochemical composition of the soils with composition data reported by Hill et al.

328 (2001) (Table 4) for the underlying basalt and the deeply weathered and lateritised basalts of the
329 Interbasaltic Formation found between the Upper and Lower Basalt Formations, shows the soils are
330 consistent with the weathered basalt, particularly the lithomarge layer from the laterite profile (Si, Ca,
331 Mg and Na are all similar). Hill et al. (2001) report that the lithomarge is predominantly comprised of
332 clays, which are mostly kaolinite and meta-halloysite at the top of the lithomarge profile, but also
333 includes a layer of "saprock" at the base of the profile that contains montmorillonite and vermiculite (Hill
334 et al., 2001).
335
336 **3.2 Mineralogy**
337 Quantitative XRD analysis determined that the amorphous content of the samples was between 65 to
338 80% (Figure 3). This very high amorphous content is likely to relate to organic materials (SOC was
339 greater than 15% for these samples) and non-crystalline weathering products such as amorphous iron
340 oxides (perhaps intergrown with clay minerals), and other precursor minerals for clays. The presence of
341 large amounts of amorphous iron oxides would explain why significant amounts of the Fe identified by
342 geochemical analysis was not identified by XRD. In their study of serpentine soils from the Czech
343 Republic, Quantin et al., (2008) also found that sequential extractions revealed significant amounts
344 (nearly 50%) of iron was present in iron (hydr)oxides that were not detected by XRD analysis.

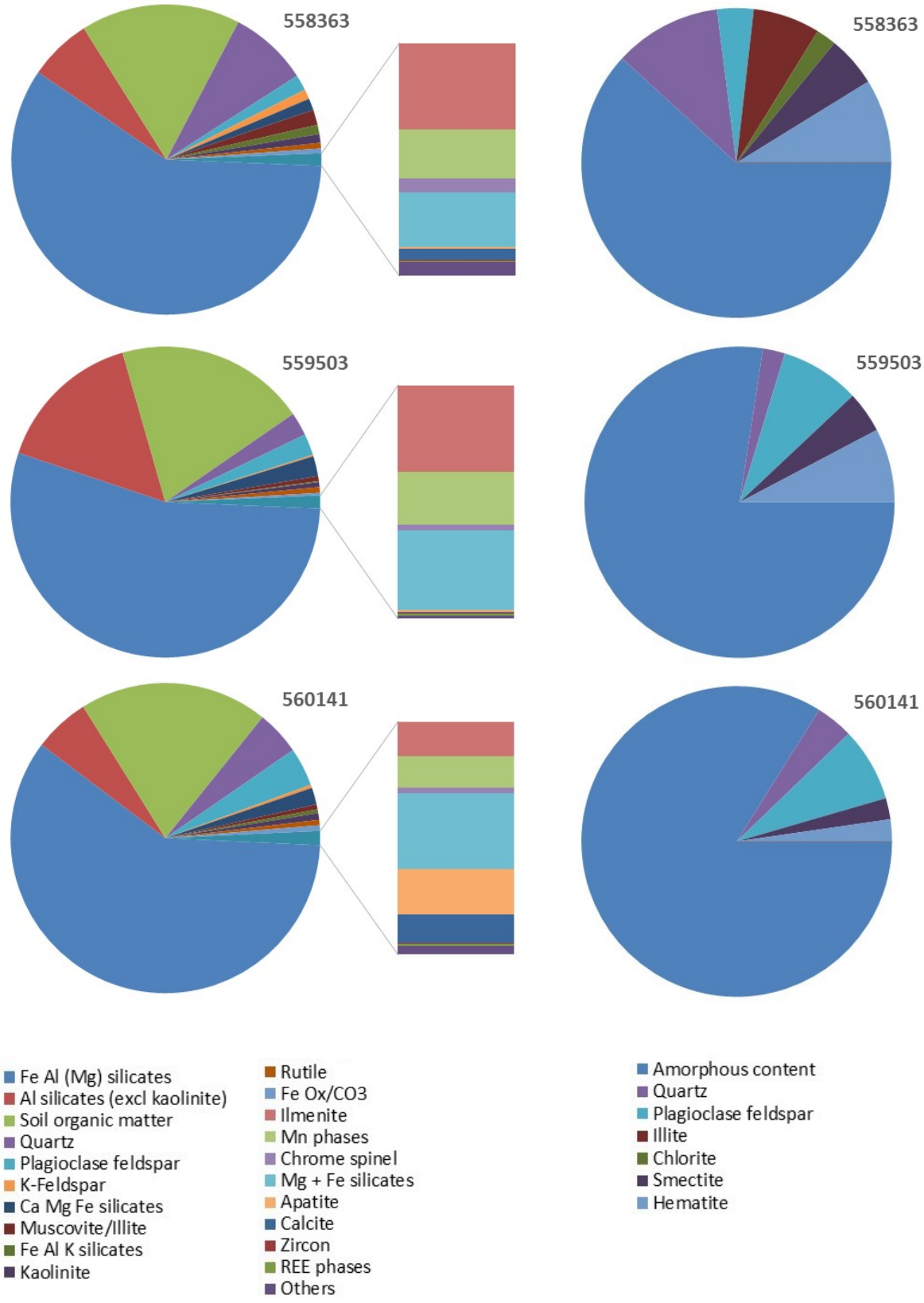

345

346 **Figure 3 Proportion of mineral components by QEMSCAN® (vol %) (left) and XRD (wt %)**

(right). For details of mineral groupings used for QEMSCAN® see Table 1.

XRD analyses also showed that smectite, illite and chlorite constitute up to 15% of the samples (Figure 3), with the greatest clay content in the sample with the lowest amorphous content (558363), suggesting this soil is more weathered than the other samples. Although the amorphous content of the sample was high and it was suspected that a significant proportion of this was 'clay like' material (including precursor clay minerals and protoclays), the percentage of soils recovered for clay XRD analysis (<2 microns) was relatively low (1-8%). Images from QEMSCAN® and EPMA showed this was because the vast majority of the agglomerations in the soil were larger than 2 microns. Clay XRD showed that 68% of clay sized particles in sample 558363 and all clay sized particles in 559503 and 560141 were found to be a randomly interstratified illite/smectite, and the remainder of the clay fraction of sample 558363 was a poorly crystalised chlorite, again supporting the hypothesis that weathering of the soils is incomplete.

QEMSCAN® analysis added further support to this hypothesis as it determined that all three samples were composed primarily of minerals initially identified as Fe Al (Mg) silicates and Al silicates (65-70%) that were often identified at the scale of individual pixels (Figure 4), suggesting they may in fact reflect amorphous protoclays of variable content. Mineral association data from QEMSCAN® supports this, as Al silicates are significantly more likely to touch Fe Al (Mg) silicates than any other mineral. Therefore from this point on, these minerals have been grouped together into an 'amorphous protoclay' group.

QEMSCAN® also identified illite (<1.58%), mica (<0.97%) and kaolinite (<0.90%), with the greatest amounts of these minerals in sample 558363.

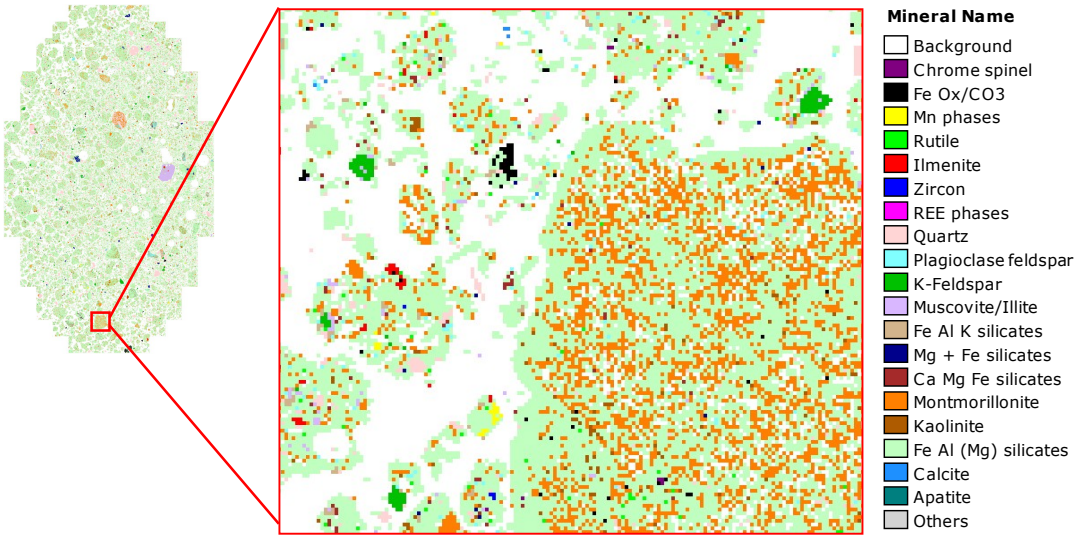

Figure 4 A typical intergrown clay grain from sample 558363

Quartz was found in all samples by both XRD (2-12%) and QEMSCAN® (2.43-8.25%) suggesting an input into the soils other than from the underlying basalts, perhaps due to movement of the glacial tills. More plagioclase feldspar was identified by XRD (3.5-8.5%) than QEMSCAN® (1.63-4.01%), however QEMSCAN® also identified K-feldspar (0.34-1.03%) and Ca Mg Fe silicates that are most likely pyroxene (1.24-2.08%). Hematite were identified by XRD, as would be expected for soils overlying basalt bedrock, however the quantities of hematite determined (2-9%) did not account for all the Fe recorded in the geochemical analysis (8-12%) supporting the suggestion that the amorphous content includes non-crystalline iron oxides. QEMSCAN® identified a variety of metal oxides and hydroxides, at trace concentrations (<0.6%). These included titanium oxides, iron oxides, ilmenite, Mn-Fe oxides and

chrome spinels. Olivine was identified by QEMSCAN® to be present at low concentrations (<0.5%) in the soil, reflecting the fact that although it is present in the underlying basalt bedrock in significant concentrations (Lyle, 1979), it is very easily weathered (Delvigne et al., 1979). Significantly more apatite (0.29%) and calcite (0.19%) were recorded in sample 560141, than the other two samples (0.01% apatite and <0.07% calcite), which supports the finding by Cox et al. (2013), using the CISED methodology, that significantly more carbonate was present in Sample 560141 than the other 2 samples.

Overall results from XRD and QEMSCAN® analyses are consistent, within the limitations of each method as set out by (Boni et al., 2013), and suggest a mineralogical makeup similar to "saprock" which Hill et al. (2001) found at the base of the lithomarge layer in the underlying Interbasaltic Formation. QEMSCAN® allowed greater characterization of the significant quantity of amorphous material in the samples than XRD, but was unable to distinguish between polymorphs. QEMSCAN® also allowed identification and mapping of trace mineralogy at concentrations below the detection limits of XRD. It should be noted that quantification analyses by XRD cannot be directly compared with measurements by QEMSCAN®, as XRD is reported in wt % whilst QEMSCAN® results refer to modal abundance (vol %), as accurate densities of each mineral were uncertain in this study and so wt % were not calculated (Boni et al., 2013).

3.3 Distribution of Cr and Ni within minerals

Ni was generally dispersed throughout element Maps 0031, 0032 and 0061 (which had the lowest

401 maximum Ni concentrations), with areas of elevated Ni concentrations associated with individual
402 minerals being more obvious in Maps 0029, 0030, 0043, 0059 and 0063 (which had the highest
403 maximum Ni concentrations). Similarly less Cr was identified in element Maps 0032 and 0061 (<900
404 mg kg^{-1}), where it was generally dispersed throughout the maps and could not be attributed to specific
405 minerals. Insignificant quantities of Cr were identified in map 0031. As Map 0029 duplicated what is
406 shown in Maps 0059 and 0063, results from Maps 0030, 0043, 0059 and 0063 are presented in Figures 5
407 to 8. All results from elemental analysis are presented as wt % of the relevant oxide.
408
409 **3.3.1** ***Chrome spinel***
410 Quantitative analysis of 11 individual points within chrome spinels revealed that concentrations of Cr
411 were typically in the range 18 to 40%. Given the proportion of chrome spinel identified in each sample
412 by QEMSCAN®, if these Cr concentrations are typical of chrome spinels in the sample, chrome spinels
413 contribute between 20 and 80% of total Cr in each sample. Fe, Al and Mg contents in chrome spinels
414 were typically 14 to 50%, 5 to 30% and 3 to 17% respectively, with Ni content being positively
415 correlated with Mg content and negatively correlated with Ca and Mn content. Si concentrations were
416 generally less than 0.02% while Ti was only elevated (9% and 14%) at two of the points identified as
417 chrome spinel. 500 to 2500 mg kg^{-1} of Ni and 1300 to 11000 mg kg^{-1} V was identified in all chrome
418 spinels. Given that chrome spinels had been investigated by point analysis, only one map (0059, Figure
419 7) was selected to include a chrome spinel, and in this case, Cr and Ni concentrations were both within
420 the range noted in the point analysis. Map 0043 (Figure 6) also revealed what appears to be a small Cr

421 spinel of Fe-Mg oxide with elevated Cr.

422

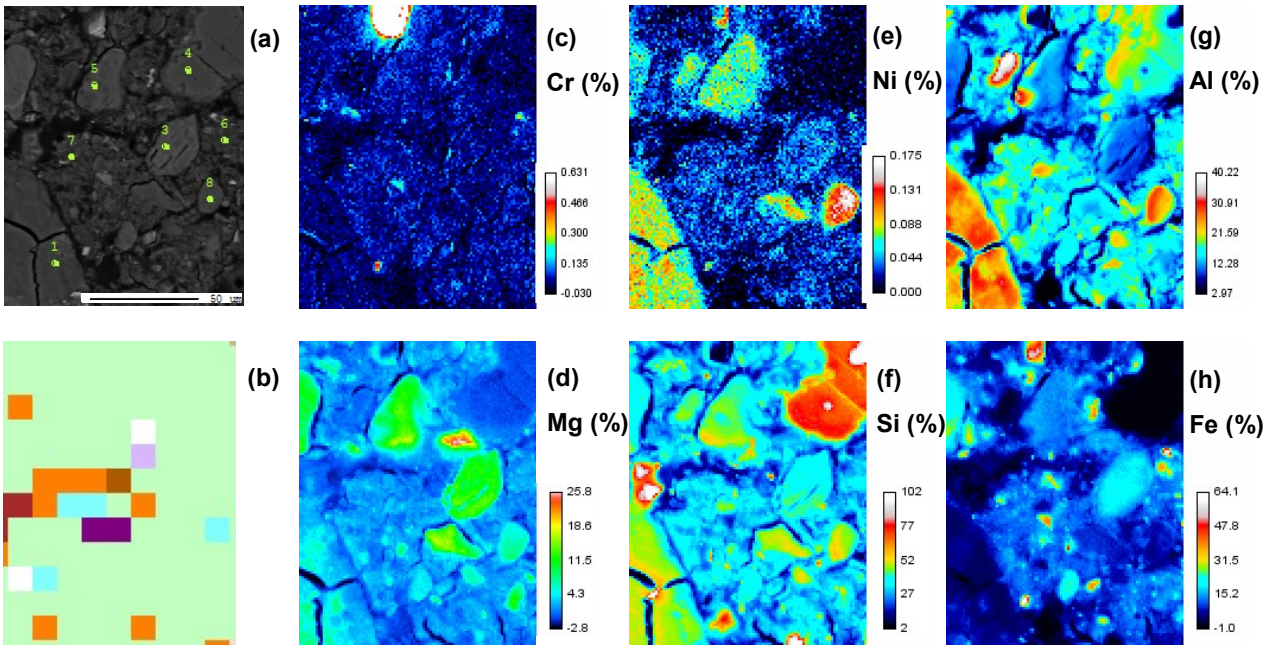

Figure 5 Detailed mapping of sample 558363 (Map 0030): (a) shows a BSE image of the map area; (b) shows mineralogical mapping of the map area (key for this map shown in Figure 4); and, (c), (d), (e), (f), (g) and (h) show elemental mapping for Cr, Ni, Al, Mg, Si and Fe.

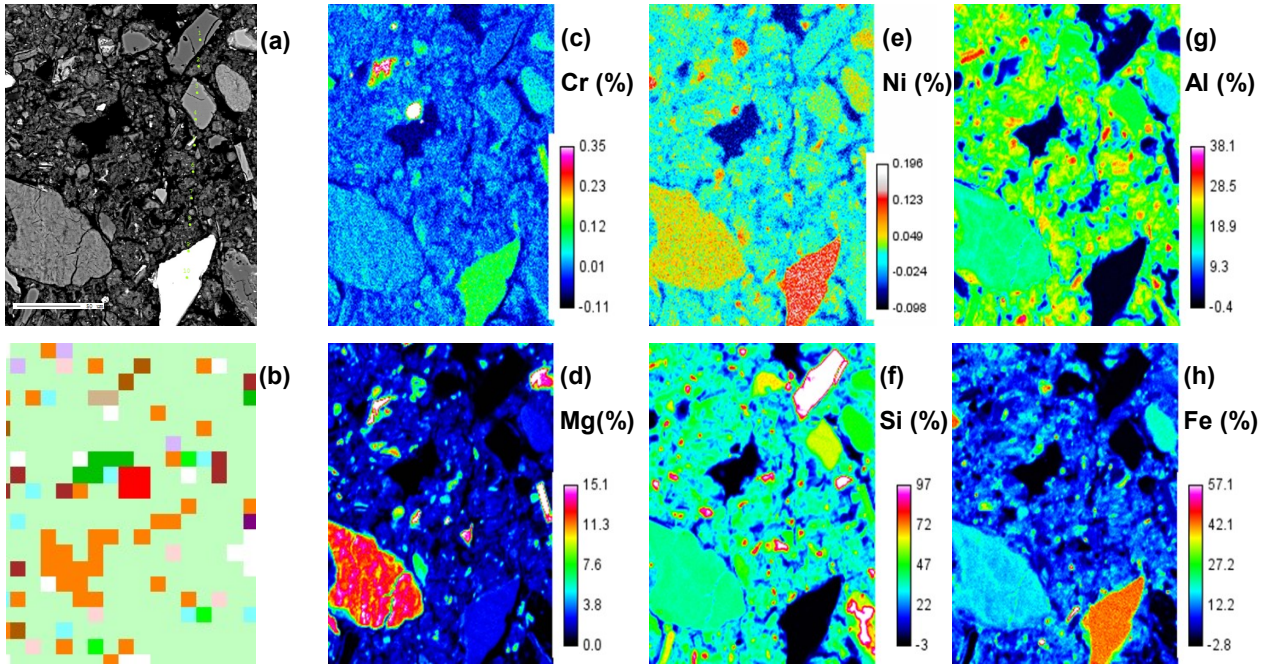

Figure 6 Detailed mapping of sample 558363 (Map 0043): (a) shows a BSE image of the map area; (b) shows mineralogical mapping of the map area (key for this map shown in Figure 4); and, (c), (d), (e), (f), (g) and (h) show elemental mapping for Cr, Ni, Al, Mg, Si and Fe.

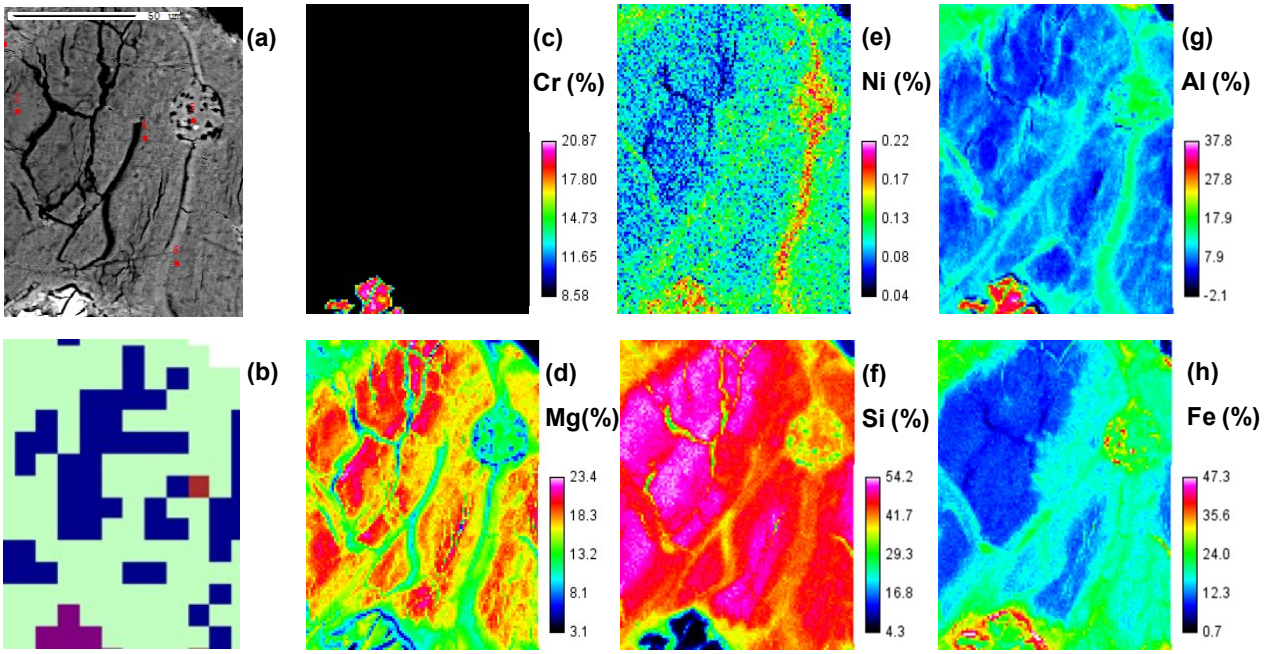

Figure 7 Detailed mapping of sample 560141 (Map 0059): (a) shows a BSE image of the map area; (b) shows mineralogical mapping of the map area (key for this map shown in Figure 4); and, (c), (d), (e), (f), (g) and (h) show elemental mapping for Cr, Ni, Al, Mg, Si and Fe.

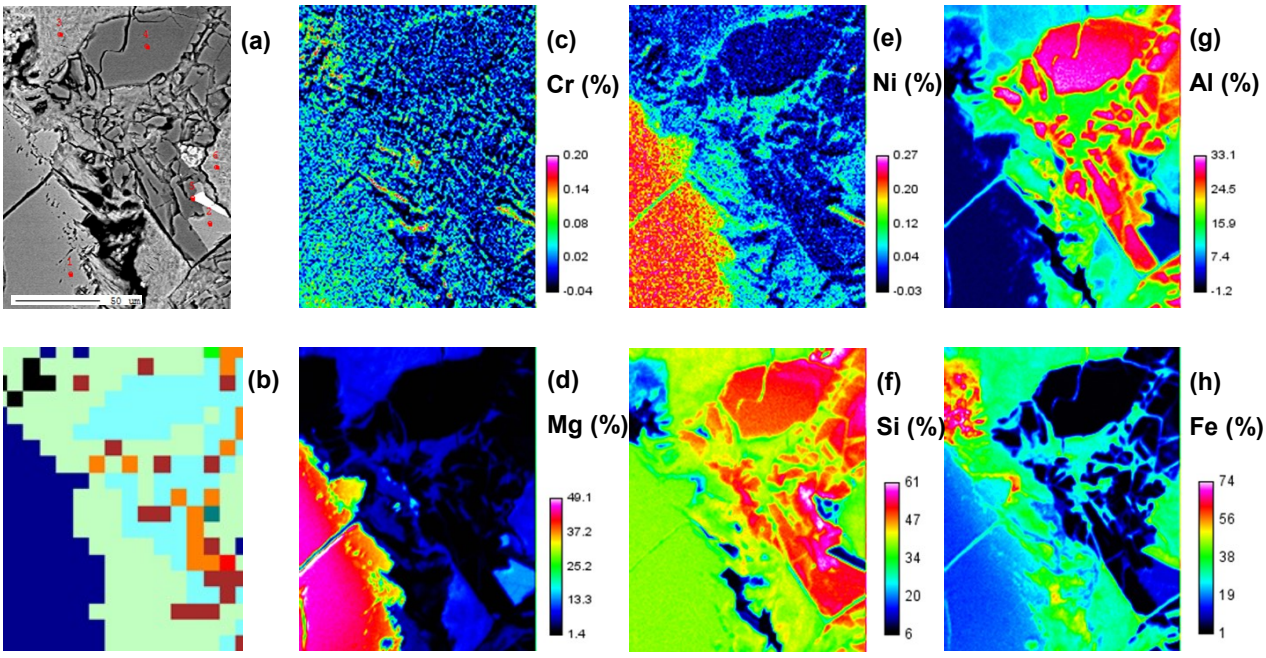

Figure 8 Detailed mapping of sample 560141 (Map 0063). (a) shows a BSE image of the map area, (b) shows mineralogical mapping of the map area (key for this map shown in Figure 4), whilst (c), (d), (e), (f), (g) and (h) show elemental mapping undertaken for Cr, Ni, Al, Mg, Si and Fe.

3.3.2 FeOx

Fe oxides were easily identified and therefore could be examined in detail using point analysis. Individual point analysis of 18 points identified as iron oxides in QEMSCAN® analysis, revealed these minerals were a combination of primary iron oxides and iron oxides intergrown with clays, that are known to be alteration products of both the weathered olivine (Delvigne et al., 1979) and pyroxene (Noack et al., 1993) that originated in the underlying basalt. Fe oxides intergrown with clays were identified by their textured appearance on BSE images and the presence of Si at concentrations of greater than 1.5%. Primary oxides by comparison had Si concentrations of <1.5% and were smooth. Generally the highest Fe concentrations (>65%) were encountered in the primary oxides, while lesser concentrations (30 to 65%) were present in intergrown oxides and clays. Cr concentrations in these minerals were generally less than 150 mg kg^{-1}, with the exception of Cr in primary iron oxides which was greater than 2000 mg kg^{-1} in two out of the four primary iron oxides tested. Ni concentrations were also generally less than 100 mg kg^{-1}, however elevated Ni concentrations (between 100 and 400 mg kg^{-1}) were identified in 5 of the 18 points tested, 4 of which were associated with intergrown oxides. Quantin et al.'s (2008) observation that only secondary Fe-Mn-oxides (and not secondary Fe-oxides) contained elevated Ni, was not confirmed in secondary iron oxides in this study as all secondary Fe-oxides contained some Ni, and Mn concentrations in none of the Fe-oxides exceed 1.5%.

Elemental mapping revealed similar results, with minerals with high Fe content not necessarily coinciding with areas of significantly elevated Cr and Ni (Figures 5 to 8). However mapping did

462 highlight a number of minerals with elevated Cr (450-2000 mg kg^{-1}) and Ni (500-1900 mg kg^{-1}) with
463 high Fe (>30%) and Ti (>10%) and zero Si concentrations. These minerals were identified as primary
464 Fe-Ti oxides. Although these minerals contained elevated Ti, inspection of Figures 5 to 8 showed Ti
465 was not necessarily correlated with either elevated Cr or Ni. No secondary iron oxides intergrown with
466 clays, containing elevated Ni or Cr were identified during elemental mapping. This was not surprising
467 as mapping did not specifically target Fe oxides identified in QEMSCAN® analysis, as these had been
468 extensively investigated by point analysis. The primary oxides noted above are very small particles that
469 were obvious due to their elevated Fe concentration.
470
471 ***3.3.3 Pyroxene***
472 Elevated Ni (500-1000 mg kg^{-1}) and Cr (500-3500 mg kg^{-1}) were identified in mineral grains in Map
473 0032 (2 No) and 0043 (Figure 6) (2 No) that contained Si (approx. 50%), Al (2-14%), Fe (5-10%), Ca
474 (8%) and Mg (10-15%), with no Na or K present. Both grains on map 0043 were identified by
475 QEMSCAN® as Ca Mg Fe silicates, but both grains on Map 0030 (Figure 5) were smaller than the
476 QEMSCAN® pixel size and were therefore not categorised. Given the underlying geology is basalt and
477 that concentrations of Si, Al, Fe, Ca and Mg fall within the range reported for pyroxenes in Deer et al.
478 (1992), it is likely that all 4 grains are pyroxene, which is known to host elevated Ni and Cr . In
479 contrast significant areas of Map 0029 were identified as Ca Mg Fe silicates by QEMSCAN®, but did not
480 contain significantly elevated Cr or Ni.
481

3.3.4 Olivine

Between 1000 and 2500 mg kg^{-1} of Ni and insignificant quantities of Cr were observed in maps 0029 and 0063 (Figure 8) in distinct areas in agglomerations within the soil matrix. These areas, that were composed of 30-40% Si, 10-35% Fe, 25-50% Mg but no Al, were identified as Mg and Fe silicates (which includes olivine) by QEMSCAN® and have a composition that is consistent with and Mg rich olivine (Deer et al., 1992). Mg rich olivine is known to host both Ni and Cr, but generally Cr is present as minute plates of chromite (Deer et al., 1992). Increasing amounts of Mg are often associated with increased Ni (Wedephol, 1978), and this is observed as 2500 mg kg^{-1} Ni was recorded in Map 0063 (Figure 8) in an area with 48% Mg and 1000 mg kg^{-1} Ni in Map 0029 in an areas with 25% Mg.

3.3.5 Clay like minerals

Clays and other clay like minerals were generally identified by visual inspection as specific grains with mottled or dappled surfaces or the secondary minerals that appear to make up the matrix in large agglomerations. Although these minerals appeared to be ubiquitous, it was impossible to visually identify which contained elevated Ni and Cr and therefore point analysis did not reveal significantly elevated concentrations of Cr and Ni in clay-like minerals. Typically concentrations of Cr and Ni identified during point analysis of clay-like grains were between 100-400 and 300-800 mg kg^{-1} respectively. In contrast mapping revealed concentrations of Ni of up to 2200 mg kg^{-1} in some claylike minerals whilst no significantly elevated Cr was identified in any of these materials, other than whisps of elevated Cr (approx. 2000 mg kg^{-1}) within what appeared to be a claylike weathering products on the

boundaries of a distinct grain of olivine in map 0063 (Figure 8) which appear to be associated with depleted Mn and Fe.

Elevated Ni concentrations (up to 2200 mg kg^{-1}) were hosted in what appeared to be clay-like materials (generally identified as as Fe Al (Mg) silicates by QEMSCAN®). This mineral contained 14-24% Si, 5-16% Al, 6-20% Fe and up to 9% Mg, with increasing Ni concentration being weakly correlated with increasing Fe. Delvigne et al. (1979) reported that during weathering in shallow media under both hydrated and oxidizing conditions, iron enters into the chlorite lattice forming a mixed structure of goethite and magnesium smectite.

Maps 0030 (Figure 5) and 0043 (Figure 6) were targeted on areas of what appeared to be agglomerations containing claylike minerals. Map 0030 shows elevated Ni (1000 to 1750 mg kg^{-1}) throughout the whole map in some of the grains that were identified as Fe Al (Mg) silicates by QEMSCAN®. A particularly large grain in the bottom left of Map 0030, hosting 1300 mg kg^{-1} of Ni, was identified as a mixture of Fe Al (Mg) silicates and kaolinite by QEMSCAN®. Less Ni was present in clay like minerals in map 0043, with a large grain, identified as Fe Al (Mg) silicates by QEMSCAN, hosting 700 mg kg^{-1} Ni and a smaller grain QEMSCAN® identified as Fe Al (Mg) silicates mixed with illite, hosting 500-600 mg kg^{-1} Ni.

Map 0059 (Figure 7) surveyed an area of what appeared to be olivine, that was in places significantly

522 weathered, enclosing a chrome spinel. Elevated Ni was encountered throughout the grain, with the lowest
523 concentrations (400-1000 mg kg^{-1}) observed in Mg rich areas (18-25% Mg) at the centre of the grain.
524 These areas have very little Al, and were identified as Mg Fe silicates by QEMSCAN® and are likely to
525 be predominantly unweathered olivine. Concentrations of Ni increase in surrounding areas, which also
526 show increased Al and Fe and decreased Mg compared with the olivine. These are identified by
527 QEMSCAN® as Fe Al (Mg) silicates and are likely to be protoclays that are initial alteration products of
528 olivine. The highest concentrations of Ni (up to 2000 mg kg^{-1}) are found in fractures within the grain
529 that also have the highest Al (up to 25%) and Fe (up to 28%) and lowest Mg (approximately 10%)
530 concentrations, suggesting Ni and Fe are accumulating in the alteration products of olivine, which are
531 likely to be clay-like minerals.
532
533 Map 0063 (Figure 8) includes an olivine grain (50% Mg) with 2500 mg kg^{-1} of Ni that is enclosed within
534 a soil grain that was shown to also include feldspars and Fe Al (Mg) silicates using QEMSCAN®. Ni is
535 present in lower concentrations (400-1000mg/kg) within a fracture in the olivine and the surrounding
536 material. These areas also have greater concentrations of Al (15%) and Fe (30%) indicating they are
537 alteration products of the olivine.
538
539 ***3.3.6 Carbonates***
540 10 analysis point were undertaken on calcite minerals and 4 analysis points were undertaken in apatite
541 minerals from sample 560141. Generally Ca concentrations ranged from 20 to 60% at these points,

542 with elevated P (30 to 35%) recorded in apatite samples. Insignificant amounts of Cr (<60 mg kg^{-1}) and
543 Ni (<90 mg kg^{-1}) were identified in all but two of these 14 samples, with 360 mg kg^{-1} of Ni found in 2
544 calcite points and 200 and 400 mg kg^{-1} of Cr found in a point analysed on apatite and a point on calcite
545 respectively. Map 0061 was selected to include areas identified as apatite during QEMSCAN® analysis,
546 however no elevated Ni or Cr was identified.
547
548 **3.4 Relation of results to oral bioaccessibility**
549 Total Ni concentrations were approximately 50% greater in samples 559363 and 559503 than in sample
550 560141, but the greatest amount of bioaccessible Ni (9.94 mg kg^{-1} (gastric phase)) was observed in
551 sample 560141. In contrast approximately 50% more total Cr was observed in sample 558383 than the
552 other 2 samples, with gastric (G) and gastrointestinal (GI) Cr showing similar trends. Total and
553 bioaccessible Ni and Cr for the three samples as measured during the Tellus survey and by Barsby et al.
554 (2012) are provided in in Table S1 in the supporting information.
555
556 Using non-specific sequential extraction (CISED) undertaken on the same soil samples, Cox et al. (2013)
557 identified carbonate, Al rich, clay and Fe oxide components that contained bioaccessible Ni.
558 QEMSCAN® analysis identified the presence of greater amount of Ca carbonates (calcite) and
559 phosphates (apatite) in Sample 560141 than the other soils (Fig. 9(b)). This supports the results of
560 previous CISED extractions (Cox et al., 2013) which attributed more bioaccessible Ni (37%) to Ca
561 dominated phases in this soil than the other 2 soils.

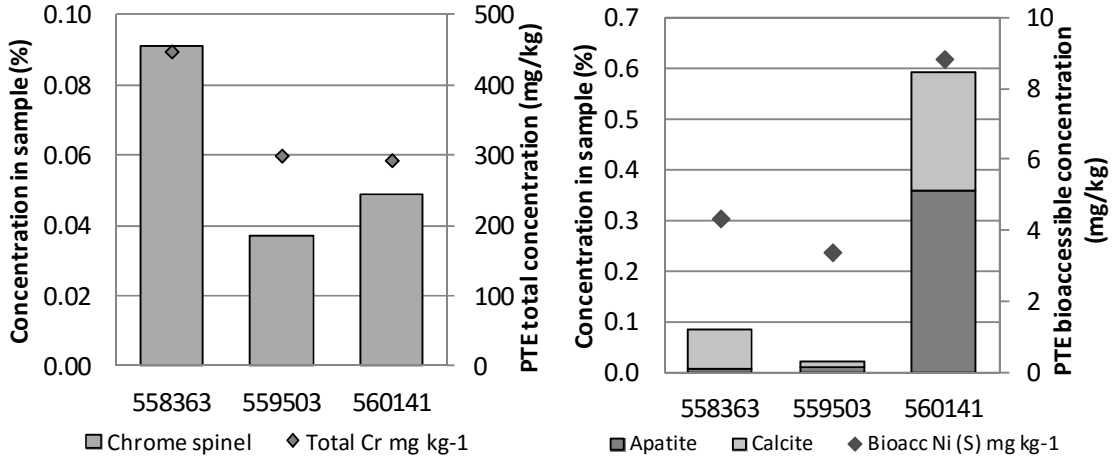

562

563 **Figure 9 Percentage composition of the trace minerals (a) chrome spinel (including chromite) and**

564 **(b) apatite and calcite (including other Ca carbonates and phosphate) plotted with (a) total Cr**

565 **concentration and (b) bioaccessible Ni concentration.**

566

567 Al-oxides were not identified by either QEMSCAN or XRD analysis in this study, suggesting that the Al

568 dominant component that contained significant amounts of bioaccessible Ni identified by Cox et al.

569 (2013) is likely to be an amorphous protoclay or precursor mineral that is dispersed within the soil matrix.

570 This precursor mineral was shown by Cox et al. (2013) not to contain bioaccessible Cr. However other

571 clays-like minerals hosted significant quantities of both bioaccessible Ni and to a lesser extent

572 bioaccessible Cr. Although they varied significantly in composition, Ni was found to accumulate in

573 many (but not all) of these clay-like minerals. Hill et al. (2001) observed similar accumulation of Ni in

574 the lithomarge within laterites in the Antrim Lava Group, which they postulated was due to substitution

575 of Ni in montmorillonite or vermiculite in the lithomarge. As substituted Ni would be readily released

576 in the stomach, Ni present in these clay-like minerals is likely to be bioaccessible.

As predicted by Cox et al. (2013) EPMA point analysis in this study identified Fe oxides with high Al and Si content that were identified as Fe oxides intergrown with clays. This intergrown oxides contained elevated Ni that would be likely to be bioaccessible. Small quantities of Cr were present in these minerals, accounting for the small amount of bioaccessible Cr identified in Fe-oxides in Cox et al. (2013).

Cox et al. (2013) reported that the majority of Cr in these soils was not bioaccessible. In this study, total chromium was found to be strongly correlated to the presence of chrome spinel in all samples (Figure 9(a)). Chrome spinels are highly recalcitrant minerals, which is reflected in the low bioaccessibility (approx 2%) for each of these samples (Cox et al., 2013). Elevated Cr concentrations were also identified in primary metal oxides which are also highly recalcitrant and therefore unlikely to contribute significantly to oral bioaccessibility. Some elevated Cr (approximately 200 to 400 mg kg^{-1}) was identified in weathered olivine and clays and some calcite and apatite, which are likely to be more bioaccessible. Cr concentrations were generally low in most calcite, apatite, feldspars and iron oxides intergrown with clays.

4.0 CONCLUSIONS

The geochemical composition of the 3 soils is similar reflecting that they overlie bedrock of similar origin. Geochemical and mineralogical data indicate the soils are consistent with the weathered basalt, particularly the "saprock" within the lithomarge layer from the laterite profile (Hill et al., 2001).

Mineralogical investigation of the samples by quantitative XRD and QEMSCAN® was generally consistent within the limitations of each method. QEMSCAN® allowed greater characterization of the significant quantity of amorphous material in the samples than XRD, but was unable to distinguish between polymorphs. QEMSCAN® also allowed rapid identification and mapping of trace mineralogy at concentrations below the detection limits of XRD. Results of both techniques indicate significant amorphous content (>60%) in the samples, which has been attributed to organic materials and non-crystalline weathering products such as amorphous iron oxides and precursor minerals for clays, suggesting that weathering of the soils is incomplete. Quartz and plagioclase feldspar were identified by both XRD and QEMSCAN®, however QEMSCAN® also identified K-feldspar, pyroxene and olivine. Hematite was identified by XRD, whilst QEMSCAN® identified a variety of metal oxides and hydroxides, at trace concentrations (<0.6%). These included titanium oxides, iron oxides, ilmenite, Mn-Fe oxides and chrome spinels. Whilst apatite and calcite were identified in all samples by QEMSCAN®, significantly more was recorded in sample 560141, than the other two samples.

Cr was identified by EPMA in chrome spinel at concentrations that could account for up to 80% of the Cr

615 in each sample. EPMA also identified up to 2000 mg kg^{-1} Cr in some primary iron oxides and up to
616 3500 mg kg^{-1} Cr in pyroxene. Surprisingly Cr was identified at concentrations of up to 400 mg kg^{-1} in 2
617 out of 14 of the apatite and calcite points investigated during point analysis by EPMA. Limited Cr was
618 identified in secondary Fe oxides, olivine and clay like minerals. The existence of the majority of total
619 Cr in highly recalcitrant chrome spinel and primary metal oxides, and to a lesser extent olivine and
620 pyroxene, explains the very low Cr bioaccessibility recorded in these samples, whilst the slightly elevated
621 Cr identified in secondary iron oxides, clay like materials, calcite and apatite is likely to be more
622 bioaccessible.
623
624 Although Ni was identified in chrome spinel (up to 2500 mg kg^{-1}), primary iron oxides (up to 1900 mg
625 kg^{-1}), Mg rich olivine (up to 2500 mg kg^{-1}) and pyroxene (up to 1000 mg kg^{-1}), Ni was distributed more
626 widely throughout the samples than Cr, with concentrations of up to 400 mg kg^{-1} identified in the
627 amorphous secondary iron oxides (especially those intergrown with clays) and concentrations of up to
628 2200 mg kg^{-1} in some of the amorphous clay-like minerals that are likely to be protoclays or precursor
629 clay minerals. Although it was impossible to visually identify which of these materials contained
630 elevated Ni, elemental mapping revealed that some elevated Ni appeared to be associated directly with
631 alteration products formed due to weathering of olivine (although this was not always the case) and
632 increasing Ni concentration appeared to be weakly correlated with increasing Fe in “clay-like” minerals.
633 The greater amount of Ni than Cr present in secondary oxides and other weathering products is likely to
634 originate from weathered olivine (which contained insignificant amounts of Cr), explaining the higher

bioaccessibility of Ni than Cr in these soils. Calcite and apatite were also found to host significant amounts of bioaccessible Ni in 1 of the 3 samples.

The combined analysis approach adopted in this investigation, utilising mineralogical analysis, elemental mapping and standard chemical analysis, allows the minerals hosting PTEs to be clearly identified, allowing increased understanding of the bioaccessibility of PTEs in soils.

5.0 ACKNOWLEDGMENTS

Geochemistry data were provided by the Geological Survey of Northern Ireland as part of the Tellus Project, which was funded by the Department of Enterprise, Trade and Investment of Northern Ireland and by the EU 'Building Sustainable Prosperity' programme of the Department of Agriculture and Rural Development. QEMSCAN® and EPMA analysis was supported by the EU INTERREG IVA-funded Tellus Border project. The authors express their thanks to Ben Buse at University of Bristol and Jonathan Wilkins at X-Ray Mineral Services for assistance with EPMA and XRD analysis.

6.0 REFERENCES

Albanese, S., Sadeghi, M., Lima, A., Cicchella, D., Dinelli, E., Valera, P., Falconi, M., Demetriades, A., De Vivo, B., 2015. GEMAS: Cobalt, Cr, Cu and Ni distribution in agricultural and grazing land soil of Europe. J. Geochemical Explor. 1–13. doi:10.1016/j.gexplo.2015.01.004

Andersen, J.C.Ø., Rollinson, G.K., Snook, B., Herrington, R., Fairhurst, R.J., 2009. Use of QEMSCAN

655 for the characterization of Ni-rich and Ni-poor goethite in laterite ores. Miner. Eng. 22, 1119–1129.
656 doi:10.1016/j.mineng.2009.03.012
657 Argyraki, A., Kelepertzis, E., 2014. Urban soil geochemistry in Athens, Greece: The importance of local
658 geology in controlling the distribution of potentially harmful trace elements. Sci. Total Environ.
659 482-483, 366–77. doi:10.1016/j.scitotenv.2014.02.133
660 Barsby, A., McKinley, J.M., Ofterdinger, U., Young, M., Cave, M.R., Wragg, J., 2012. Bioaccessibility of
661 trace elements in soils in Northern Ireland. Sci. Total Environ. 433, 398–417.
662 doi:10.1016/j.scitotenv.2012.05.099
663 Boni, M., Rollinson, G., Mondillo, N., Balassone, G., Santoro, L., 2013. Quantitative Mineralogical
664 Characterization of Karst Bauxite Deposits in the Southern Apennines, Italy. Econ. Geol. 108,
665 813–833.
666 Cave, M.R., Wragg, J., Denys, S., Jondreville, C., Feidt, C., 2011. Oral Bioavailability, in: Swartjes, F.A.
667 (Ed.), Dealing with Contaminated Sites. Springer Netherlands, pp. 287–324.
668 doi:10.1007/978-90-481-9757-6_7
669 Chartered Institute of Environmental Health (CIEH), 2009. Professional Practice Note: Reviewing
670 human health risk assessment reports invoking contaminant oral bioavailability measurements or
671 estimates.
672 Colin, F., Nahon, D., Trescases, J.J., Melfi, A.J., 1990. Lateritic Weathering of Pyroxenites at
673 Niquelandia, Goias, Brazil: The Supergene Behavior of Nickel. Econ. Geol. 85, 1010–1023.
674 Costa, C., Reis, A.P., Ferreira da Silva, E., Rocha, F., Patinha, C., Dias, A.C., Sequeira, C., Terroso, D.,

675 2011. Assessing the control exerted by soil mineralogy in the fixation of potentially harmful
676 elements in the urban soils of Lisbon, Portugal. Environ. Earth Sci. 65, 1133–1145.
677 doi:10.1007/s12665-011-1362-8
678 Cox, S.F., Chelliah, M., Mckinley, J.M., Palmer, S., Ofterdinger, U., Young, M., Cave, M.R., Wragg, J.,
679 2013. The importance of solid-phase distribution on the oral bioaccessibility of Ni and Cr in soils
680 overlying Palaeogene basalt lavas, Northern Ireland Siobhan. Environ. Geochem. Health 35,
681 553–567. doi:10.1007/s10653-013-9539
682 Cruickshank, J.G., 1997. Soil and Environment: Northern Ireland. Agricultural and Environmental Scince
683 Division, DANI and The Agricultural and Environmental Science Department, The Queen's
684 University of Belfast, Belfast.
685 Deer, W.A., Howie, R.A., Zussman, J., 1992. An introduction to rock forming minerals, second. ed.
686 Delvigne, J., Bisdom, E.D.A., Sleeman, J., Stoops, G., 1979. Olivines, their pseudomorphs and secondary
687 products. Pedologie 29, 247–309.
688 Denys, S., Caboche, J., Tack, K., Rychen, G., Wragg, J., Cave, M., Jondreville, C., Feidt, C., 2012. In
689 vivo validation of the unified BARGE method to assess the bioaccessibility of arsenic, antimony,
690 cadmium, and lead in soils. Environ. Sci. Technol. 46, 6252–60. doi:10.1021/es3006942
691 EFSA Panel on Contaminants in the Food Chain, 2015. Scientific Opinion on the risks to public health
692 related to the presence of nickel in food and drinking water. EFSA J. 13, 4004–4202.
693 Gottlieb, P., Wilkie, G., Sutherland, D., Ho-Tun, E., Suthers, S., Perera, K., Jenkins, B., Spencer, S.,
694 Butcher, A., Rayner, J., 2000. Using Quantitative Electron Microscopy for Process Mineralogy

695 Applications. JOM April, 24–25.

696 Haberlah, D., Strong, C., Pirrie, D., Rollinson, G.K., Gottlieb, P., Botha, P., Butcher, A., 2011. Automated

697 petrography applications in quaternary science. Quat. Australas. 28, 3–12.

698 Hill, I.G., Worden, R.H., Meighan, I.G., 2001. Formation of interbasaltic laterite horizons in NE Ireland

699 by early Tertiary weathering processes. Proc. Geol. Assoc. 112, 339–348.

700 doi:10.1016/S0016-7878(01)80013-4

701 Kelepertzis, E., Stathopoulou, E., 2013. Availability of geogenic heavy metals in soils of Thiva town

702 (central Greece). Environ. Monit. Assess. doi:10.1007/s10661-013-3277-1

703 Kierczak, J., Neel, C., Bril, H., Puziewicz, J., 2007. Effect of mineralogy and pedoclimatic variations on

704 Ni and Cr distribution in serpentine soils under temperate climate. Geoderma 142, 165–177.

705 doi:10.1016/j.geoderma.2007.08.009

706 Lyle, P., 1979. A petrological and geochemical study of the tertiary basaltic rocks of Northeast Ireland. J.

707 Earth Sci. 2, 137–152.

708 McIlwaine, R., Cox, S.F., Doherty, R., Palmer, S., Ofterdinger, U., McKinley, J.M., 2014. Comparison of

709 methods used to calculate typical threshold values for potentially toxic elements in soil. Environ.

710 Geochem. Health 36, 953–971. doi:10.1007/s10653-014-9611-x

711 Mitchell, W.I., 2004. The Geology of Northern Ireland Our Natural Foundation, (2004). Belfast.

712 Nathanail, P.C., McCafferty, C., Gillett, A.G., Ogden, R.C., Nathanail, J.F., 2015. The LQM/CIEH S4ULs

713 for Human Health Risk Assessment. Nottingham, UK.

714 Noack, Y., Colin, F., Nahon, D., Delvigne, J., Michaux, L., 1993. Secondary-mineral formation during

715 natural weathering of pyroxene: Review and thermodynamic approach. Am. J. Sci. 293, 111–134.
716 Palmer, S., Cox, S.F., McKinley, J.M., Ofterdinger, U., 2014. Soil-geochemical factors controlling the
717 distribution and oral bioaccessibility of nickel, vanadium and chromium in soil. Appl. Geochemistry
718 51, 255–267. doi:10.1016/j.apgeochem.2014.10.010
719 Pirrie, D., Rollinson, G.K., 2011. Unlocking the applications of automated mineral analysis. Geol. Today
720 27, 226–235.
721 Quantin, C., Ettler, V., Garnier, J., Sebek, O., 2008. Sources and extractibility of chromium and nickel in
722 soil profiles developed on Czech serpentinites. Surf. Geosci. 340, 872–882.
723 doi:10.1016/j.crte.2008.07.013
724 Rollinson, G.K., Andersen, J.C.Ø., Stickland, R.J., Boni, M., Fairhurst, R., 2011. Characterisation of
725 non-sulphide zinc deposits using QEMSCAN. Miner. Eng. 24, 778–787.
726 doi:10.1016/j.mineng.2011.02.004
727 Ruby, M. V., Schoof, R.., Brattin, W., Goldade, M., Post, G., Harnois, M., Mosby, D.E., Casteel, S.W.,
728 Berti, W., Carpenter, M., Edwards, D., Cragin, D., Chappell, W., 1999. Critical Review Advances in
729 Evaluating the Oral Bioavailability of Inorganics in Soil for Use in Human Health Risk Assessment.
730 Environ. Sci. Technol. 33, 3697–3705.
731 Santoro, L., Boni, M., Rollinson, G.K., Mondillo, N., Balassone, P., Clegg, A.M., 2014. Mineralogical
732 characterization of the Hakkari nonsulfide Zn (Pb) deposit (Turkey): The benefits of QEMSCAN.
733 Miner. Eng. 69, 29–39. doi:10.1016/j.mineng.2014.07.002
734 Smyth, D., 2007. Methods used in the Tellus Geochemical Mapping of Northern Ireland. Keyworth,

735 Nottingham.

736 Vasiluk, L., Dutton, M.D., Hale, B., 2011. In vitro estimates of bioaccessible nickel in field-contaminated

737 soils, and comparison with in vivo measurement of bioavailability and identification of mineralogy.

738 Sci. Total Environ. 409, 2700–6. doi:10.1016/j.scitotenv.2011.03.035

739 Wedephol, K.H., 1978. Spring Handbook of geochemistry. Berlin.

740 Wragg, J., Cave, M., Basta, N., Brandon, E., Casteel, S., Denys, S., Gron, C., Oomen, A., Reimer, K.,

741 Tack, K., Van de Wiele, T., 2011. An inter-laboratory trial of the unified BARGE bioaccessibility

742 method for arsenic, cadmium and lead in soil. Sci. Total Environ. 409, 4016–30.

743 doi:10.1016/j.scitotenv.2011.05.019

744 Wragg, J., Cave, M., Gregory, S., 2014. The Solid Phase Distribution and Bioaccessibility of Arsenic,

745 Chromium, and Nickel in Natural Ironstone Soils in the UK. Appl. Environ. Soil Sci. 2014, 1–12.

746 doi:10.1155/2014/924891

747

748

749

750

751

752 **Supporting information**

	558363	559503	560141
Total Ni by XRF (mg kg^{-1})	174.50	166.50	121.60
Bioacc Ni (G) (mg kg^{-1})	4.34	3.39	8.84
Ni BAF (G) (%)	2.49	2.04	7.27
Bioacc Ni (GI) (mg kg^{-1})	2.45	1.80	5.00
Ni BAF (GI) (%)	1.41	1.08	4.11
Total Cr by XRF (mg kg^{-1})	447.70	299.70	293.10
Bioacc Cr (G) (mg kg^{-1})	9.20	4.54	3.20
Cr BAF (G) (%)	2.06	1.51	1.09
Bioacc Cr (GI) (mg kg^{-1})	7.39	3.00	1.83
Cr BAF (GI) (%)	1.65	1.00	0.62

Table S1 Total Ni and Cr concentrations measured by XRF during the Tellus survey and bioaccessible Ni and Cr concentrations measured using the UBM method by Barsby et al. (2012).